Integrative and Comparative Biology

Integrative and Comparative Biology, volume 00, pp. 1–15
https://doi.org/10.1093/icb/icaf139

Society for Integrative and Comparative Biology

COMPLEMENTARY SESSION PAPER

Three-Dimensional Tracking Method for Water-Hopping Mudskippers in Natural Habitats

Daehyun Choi [*], Kai Yung [*], Ian Bergerson [*], Halley Wallace [*], Ulmar Grafe [†] and Saad Bhamla [*,1]

[*]School of Chemical and Biomolecular Engineering, Georgia Institute of Technology, 311 Ferst Dr NW, Atlanta, GA 30332, USA; [†]Environmental Life Sciences Program, Universiti Brunei Darussalam, Tungku Link Road, BE1410 Gadong, Brunei

[1]E-mail: saadb@chbe.gatech.edu

Synopsis We present a portable, noninvasive, and low-cost three-dimensional tracking method to quantify *in situ* water-hopping kinematics of mudskippers. By combining dual-camera video recordings with tracking the fish path, Gaussian Splatting terrain reconstruction and stereo matching, we capture detailed 3D trajectories of mudskippers in their natural tidal-flat habitats. Our proposed method resolves hopping motions including both straight and curved escape paths, and reveals that horizontal stride length, hopping height, and velocity are strongly influenced by fish length and local terrain features. These results highlight both the biomechanical and ecological significance of water-hopping in mudskippers, demonstrating how a simple, deployable 3D approach can resolve complex amphibious movements in challenging field environments.

Introduction

Mudskippers are uniquely adapted amphibious fish capable of dynamic terrestrial and aquatic locomotion (Fig. 1). Their ability to move on land has been extensively studied (Jaafar and Murdy 2017; Naylor and Kawano 2022; Liu et al. 2023), yet data on hopping behavior over water remain sparse (Fig. 1C). Although a few studies have mentioned this behavior in laboratory conditions (Swanson and Gibb 2004) and *in situ* (Wicaksono et al. 2020), a comprehensive analysis of their three-dimensional kinematics while interacting with their heterogeneous environment has not, to our knowledge, yet been performed. Early documentation of mudskipper locomotion can be traced back to Petit (1921) and Lee et al. (1995), who noted that each bound is preceded by a brief period of swimming, describing it as "ricochet." Harris (1960) later termed the behavior "skimming," emphasizing that the mudskipper actively powers its series of hops across the water using its caudal fin, rather than its hops being a passive bounce like a skipping stone across the surface of water (Stebbins and Kalk 1961; Rosellini et al. 2005). Harris described the skimming sequence in detail: (1) the fish swims normally with its eyes and part of its head above water, (2) it accelerates to exit the water at about a 30° angle with respect to the water surface, (3) it remains airborne, and (4) it lands back on the water surface. Harris reported an average velocity of 2.5, m s^{-1} for a 14 cm body length, corresponding to 17.9 BL s^{-1} (where BL denotes body length). Based on qualitative observations, Harris suggested that the mudskipper does not leverage its pectoral fins. However, recent imaging reveals that pectoral fins are actively used and are crucial for skimming dynamics (Pace and Gibb 2009; Wicaksono et al. 2020). From this point on, we describe this behavior as "hopping." Although this behavior is often featured in popular media (e.g., KBS Environmental Special "Wild Journey - The Mud Flat is Alive," 2019), Wicaksono et al. (2020) provided one of the first detailed kinematics report of mudskipper locomotion, classifying mudskipper hopping as a novel form of fish locomotion distinct from water-jumping or the gliding of flying fish. By using portable cameras, they documented hopping, taxiing, submergence, and combinations thereof on land, water surfaces, and tree roots, reporting velocities, time durations, and energy-loss analyses. However, using a single-camera approach inherently loses in-plane motion information.

Advance Access publication August 6, 2025

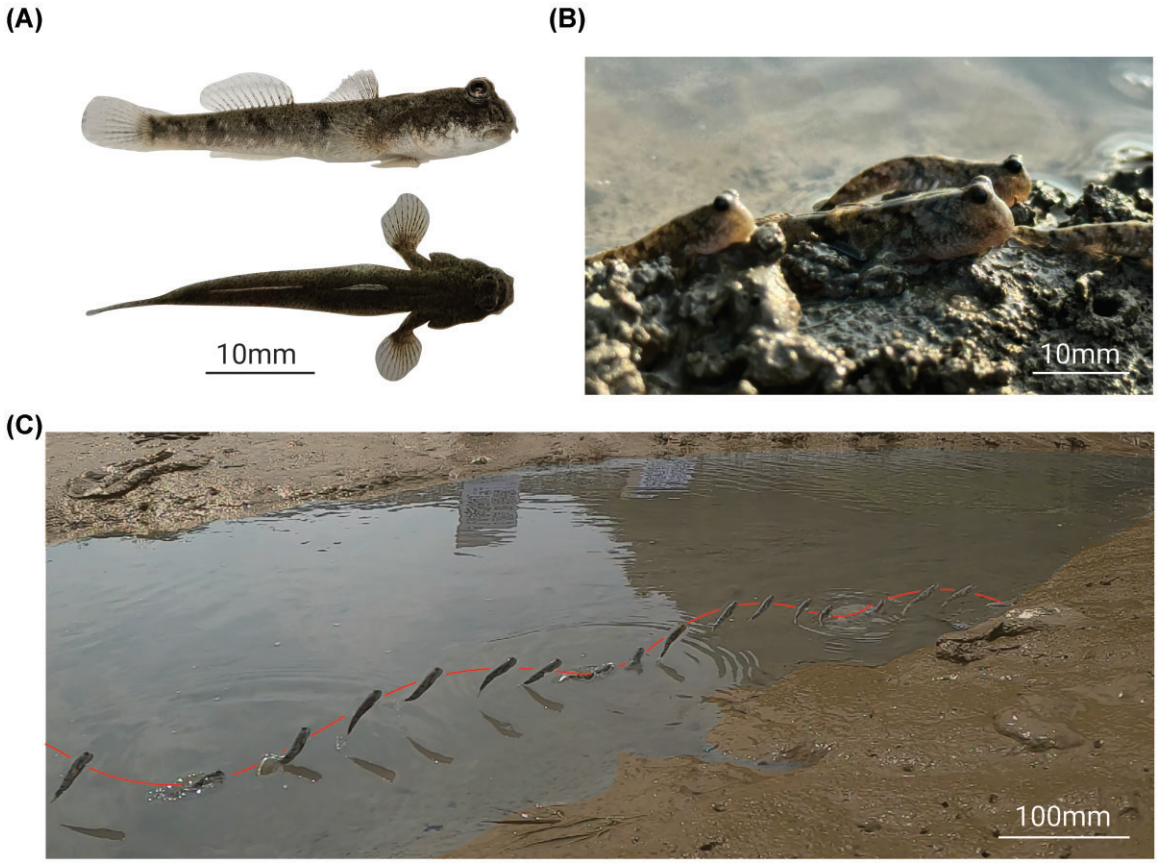

Fig. 1 *Periophthalmus modestus* in natural habitat (Daebudo, South Korea). (**A**) Side view (top) and top view (bottom) of live mudskipper. The pectoral fin is retracted in side view while extended in top view. (**B**) Mudskippers resting on the bank. (**C**) Time sequence of a mudskipper hopping across the water surface, moving left to right and landing on the bank at the right. Time intervals are uneven, selected for clarity.

In other organisms, 3D measurement techniques for the air–water interface locomotion have been used in a lab (Glasheen and McMahon 1996) or field (Weiss 2023). The basilisk lizard study (Hsieh, 2003) used a laboratory stereo rig with a fixed 90° baseline and rigid calibration frames, a setup that is difficult to implement in field conditions where the terrain is uneven and obstacles such as trees or lack of structural support prevent rigid installations. The skimming frog study (Weiss 2023) used stereo imaging with automated calibration via easyWand (Theriault et al. 2014), cutting setup time to ∼15–20 min; however, it does not capture terrain information and it can fail for certain camera poses, as calibration relies on the animal's appearance in each camera's field of view, which is difficult to constrain. Recently, advances in 3D reconstruction algorithms have facilitated the use of low-cost sensors for capturing high-resolution data. Fan et al. developed Water-Adapted 3D Gaussian Splatting for underwater terrain reconstruction, achieving PSNR of 30.43 through complexity-adaptive point distribution, although their method does not capture animal behavior or movement dynamics (Fan et al. 2025). Francisco *et al.* combined deep-learning tracking with Structure-from-Motion photogrammetry for aquatic animal tracking, achieving 1.09 ± 0.47 cm accuracy, but requiring multiple synchronized cameras and controlled lighting conditions (Francisco et al. 2020). Vieira et al. used stereo-video with two synchronized cameras for high-resolution ocean wave measurements, but the applicability was limited to nearshore environments with adequate visibility (Vieira et al. 2025). Table 1 compares the technical specifications of existing multicamera systems for 3D locomotion tracking, including measurement volumes, spatial/temporal resolution, deployment requirements, terrain reconstruction capabilities, and analytical methodologies.

Here, we introduce a novel, low-cost, and highly portable 3D tracking method for natural habitats using two cameras, which combines an existing 3D Gaussian Splatting (using the commercial software PolyCam [Kerbl et al. 2023; 3D Polycam Inc 2024]) with 3D camera ray reconstruction using in-house code. Here, the camera ray is the 3D line passing through the camera center and the image point. This study provides two main contributions. First, we detail our field-

Table 1 Technical specifications of multi-camera systems for 3D animal locomotion tracking.

Study	Animals (environment)	Measurement volume	Spatial resolution or error (frame rate)	Setup requirements (installation time)	Terrain info.	Methodology
Hsieh (2003)	Basilisk lizards (indoor water track)	0.34 m (L) × 0.11 m (W) × 0.18 m (H)	±0.2 mm error (250 fps)	Fixed two cameras (-)	No	Conventional DLT
Theriault et al. (2014)	Bats and birds (aerial space around colony)	O(10) m × O(10) m × O(10) m	7–10 mm/px (∼100 fps)	Flexible placement of three cameras (45 min)	No	SBA
Weiss (2023)	Cricket frogs (outdoor pond)	3.0 m (L) × 3.0 m (W)∗	±10 mm error (60–2000 fps)	Flexible placement of five cameras (15–20 min)	No	SBA
Francisco et al. (2020)	Fish (natural aquatic environments)	Up to 500 m^2 area	10.9 ± 4.7 mm RMSE tracking error (30–60 Hz)	2–12 sync cameras (-)	Yes	Deep learning + SfM
Vieira et al. (2025)	Ocean waves (nearshore ocean)	20 m (L) × 30 m (W)∗	1.9–17.5 mm RMSE (12 fps)	Flexible placement of three cameras (15–20 min)	No	WASS; low cost
Fan et al. (2025)	- (underwater environment)	-	- (-)	- (-)	Yes	3D Gaussian Splatting
Choi et al. (This work)	Mudskippers (natural tidal habitats)	1.5 m (L) × 1.5 m (W) × 1.0 m (H)	0.27–0.64 mm/px (240 fps)	Flexible placement of two cameras (25 min)	Yes	3D Gaussian Splatting; low cost

L = length; W = width; H = height; px = pixels; fps = frames per second; RMSE = root mean square error; SBA = Sparse Bundle Adjustment; SfM = Structure from Motion; DLT = Direct Linear Transformation; WASS = Wave Acquisition Stereo System. ∗Height not specified; - Not specified.

ready 3D imaging technique that allows unobtrusive monitoring of amphibious fish in their native environment. Second, we demonstrate that our method yields high fidelity motion trajectories, enabling high spatio-temporal resolution measurement with a spatial resolution of 0.27−0.64 mm near the center of the field of view (FoV) (which may vary depending on camera configuration, pixel location, lens distortion, and ray angle relative to the centerline) and a temporal resolution of 4.17ms, for analyzing interfacial hopping performance within a wide FoV of ∼1.5 × 1.5 × 1.0 m in the x, y (horizontal), and z (gravity) directions, respectively. Overall, our results highlight the efficacy of non-invasive, three-dimensional tracking as a powerful tool for studying the biomechanics and ecology of amphibious animals in their natural environments.

Method

Location selection

We selected two tidal flat areas on two islands (Daebudo in South Korea and Bedukang in Brunei) for the observation of two mudskipper species: *Periophthalmus modestus* and *Periophthalmus gracilis*. Mudskippers mainly inhabit brackish areas, where seawater and freshwater meet. Ikebe and Oishi observed the same species, *P. modestus*, as shown in Fig. 1, while studying their behavior during high tide (Ikebe and Oishi 1996) and documented earlier by Macnae (1969). After identifying a few possible mudskipper sighting locations through internet search, we conducted a preliminary site survey and interviews with local residents 1 and 2 days before the observation date. We selected these sites based on the sufficient presence of mudskippers (Fig. 1B), as well as their safety and accessibility for field research. Daebudo Island is located near private land right next to a road, and in Brunei, we hired a captain to reach the uninhabited island of Bedukang. For reference, the Brunei trip was preapproved by the authorities (approval number: UBD/AVC-RI/1.21.1[a]/2024/009). Coordinates and experiment date for both sites are provided in Acknowledgments.

The observation area was located where freshwater flows into the sea (estuarine zone, see Fig. 2B), where the high population density of mudskippers was during field research (Fig. 1B). Due to the tidal effect, the sea level changes over time (Figs. 2A and C) and this area becomes completely submerged during high tide (Fig. 2D). Therefore, we limited the maximum observation time to 3 h and had to develop a methodology to complete all the experiments within that period.

Camera configuration and measurement setup

The locomotion of the mudskippers on site was captured by two tripod-mounted portable cameras (GoPro Hero 10 and Hero 12) with a resolution of 2704 × 1520 pixels (2.7k) at 240 fps for both cameras (Fig. 3A). An additional handheld portable camera (Samsung Galaxy 23, 50MP resolution) was used to capture terrain snapshots for 3D surface reconstruction (Fig. 3A). Two calibration targets (Fig. 3A) were used to calibrate the length scale and camera orientation; implementation details are discussed later. The entire setup is low-cost (under $1500 at current market prices) and portable, allowing a single observer to carry and operate it in the field (Fig. 3B).

Experimental procedure and data acquisition

The experimental steps were as follows:

(1) We first selected sites that were both mudskipper-dense and suitable for camera setup.
(2) Camera 1, Camera 2, and the calibration targets were positioned (see Fig. 4A), and recording was initiated (∼5 min).
(3) Terrain snapshots were then taken from multiple angles (Fig. 4B) using a third portable camera (additional 5 min).
(4) Cameras 1 and 2 recorded simultaneously for 15 min, while the operator gently provoked mudskippers by waving a long stick or hand from a distance, without physical contact, to trigger escape responses.
(5) After recording, equipment was removed, and the procedure was repeated at two additional sites (three trials each for Daebudo and Bedukang).

Each installation and recording session lasted ∼25 min, allowing all measurements to be completed, sufficiently, within 2 h during low tide.

Terrain reconstruction using gaussian splatting

To capture three-dimensional terrain information, multiple snapshots were taken from various angles using a 50MP high-resolution camera (Samsung Galaxy 23) (Fig. 4B). Using these images, Gaussian splatting algorithm (PolyCam, 3D Polycam Inc 2024) generated 3D point clouds and reconstructed the terrain surface (Fig. 4C). The resulting terrain data also includes the positions of the cameras, allowing for flexible camera placement during experiments. To improve accuracy, the camera positions and orientations were further refined. A virtual camera was placed at the experimental camera locations within the reconstructed terrain to generate synthetic images (see two cameras in Fig. 4F). By aligning the observed calibration pattern (left side of Fig. 4D) with the reconstructed one (right side of Fig. 4D), camera orientation and focal length could be fine-tuned (see comparisons in Fig. 4D and E).

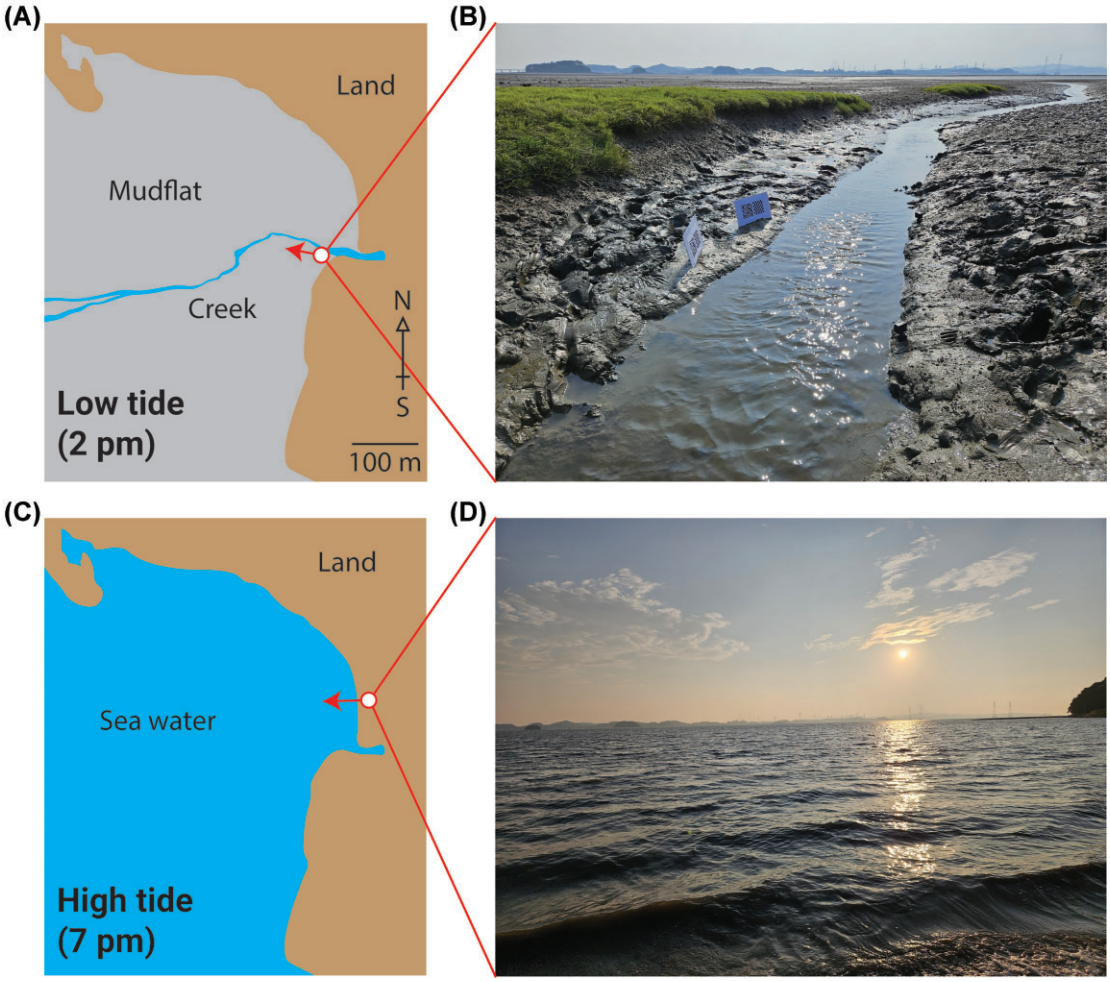

Fig. 2 Natural habitat of mudflat area in Daebudo, South Korea. (**A**, **C**) Topographies and (**B**, **D**) images of mudflat area: (**A**, **B**) low tide and (**C**, **D**) high tide. The solid arrows in (**A**) and (**C**) indicate the camera direction for images (**B**) and (**D**), respectively. See Acknowledgments for detailed location and date.

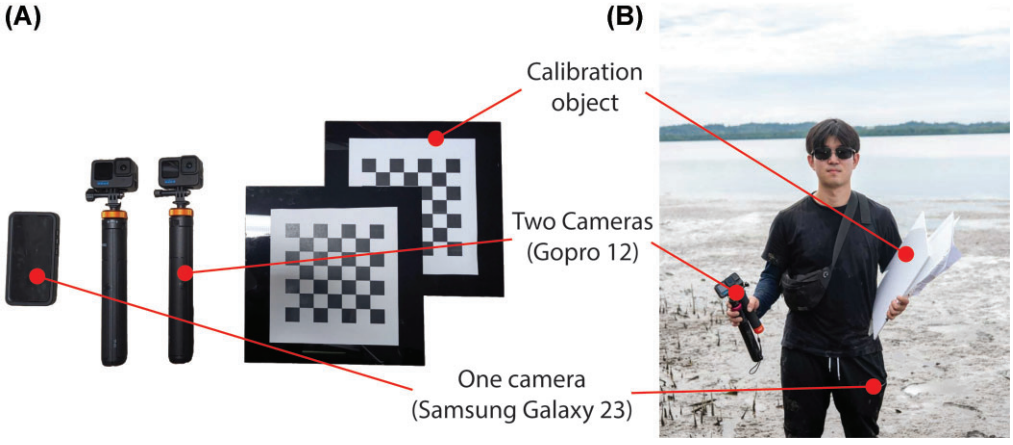

Fig. 3 (**A**) Experiment equipment (two action cameras [GoPro] mounted with tripods, one cell phone, and two calibrations targets) and (**B**) carrying demonstration in field (Pulau Bedukang). Image includes the first author, with permission granted for publication.

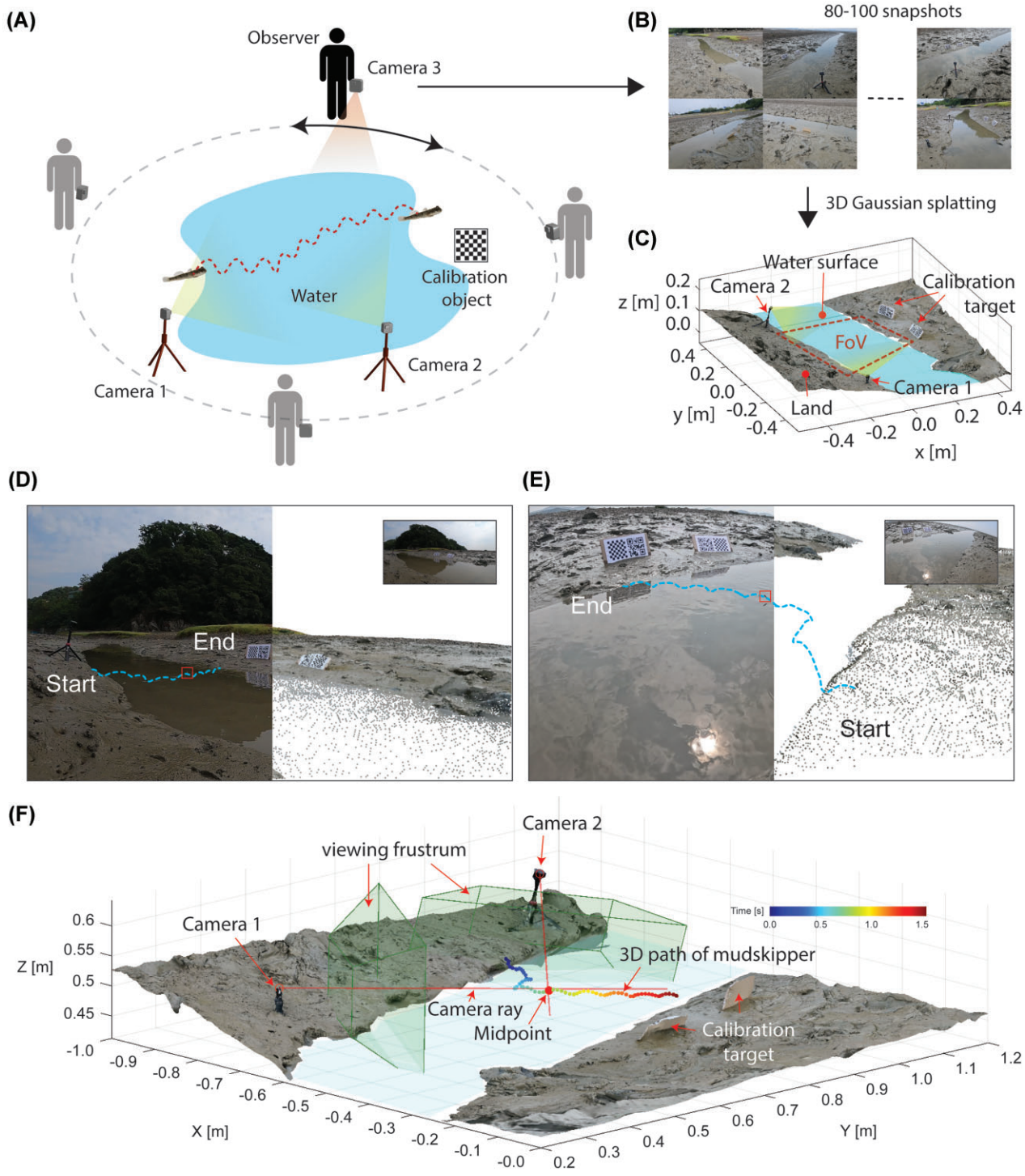

Fig. 4 Method to obtain the 3D trajectory of mudskipper. (**A**) Measurement setup. (**B**) Raw image of snapshots for local terrain. (**C**) The reconstructed 3D terrain from 3D Gaussian splatting. (**D**, **E**) Camera view (left part) and the virtual camera view (right part) from (**D**) left and (**E**) right camera. (**F**) The reconstructed 3D trajectory from both cameras. Here, two camera rays are indicated in red and camera intrinsics such as focal depth and focal angle are visualized by frustums.

Estimation of 3D trajectory

To obtain the mudskipper's three-dimensional position, time-series trajectories were first tracked in each camera view using DLTdv8 (Hedrick 2008), yielding pixel coordinates (see Fig. 4D and E, where the trajectory is shown as a dotted line and instantaneous positions are marked with red boxes). Here, the midpoint between the mudskipper's eyes was tracked, as

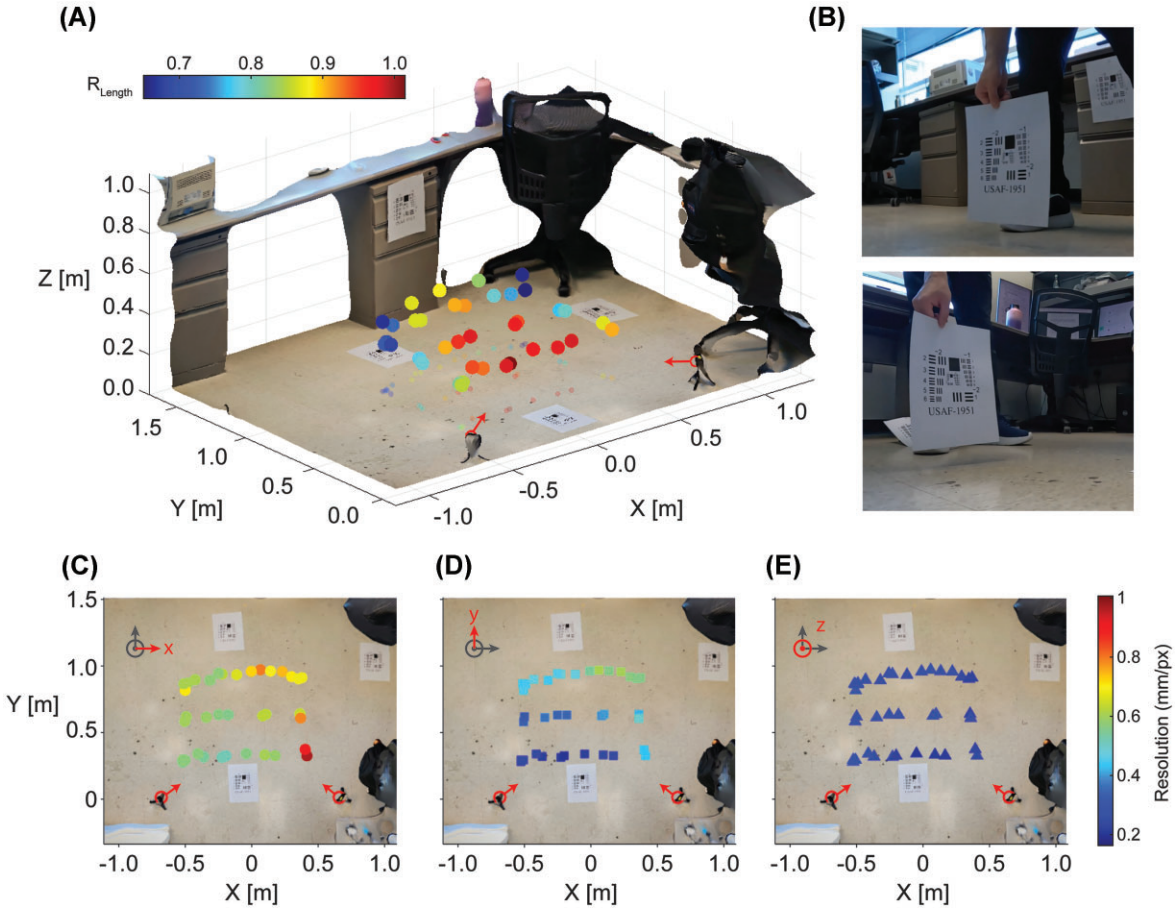

Fig. 5 Validation of stereo imaging system. (**A**) 3D locations and length ratio between measured and actual length of square elements in USAF-1951 target. (**B**) Field of view of both cameras showing custom USAF- 1951 target. (**C**–**E**) Directional resolution (mm/pixel) in *x*, *y*, and *z* directions, respectively.

the eyes are generally exposed to air and thus consistently visible to the camera. The sampling interval between trajectory points was 5 frames (i.e., 0.021 s at a 240 Hz frame rate), and a total of $n = 33$ trajectories across the three trials were extracted for statistics (Fig. 5).

With fine-tuned focal lengths, camera positions, and orientations, each trajectory point was mapped onto its corresponding camera ray within the 3D virtual terrain (red lines in Fig. 4F). The intersection of the two camera rays from the stereo pair represents the mudskipper's 3D location. Due to minor errors in camera parameters and tracking data, the rays did not intersect exactly; thus, the 3D position was approximated by computing the midpoint of the closest pair of points on the two skew lines. All computations including importing 3D terrain data (OBJ format), generating camera rays, and calculating midpoints were performed in MATLAB (R2022B) using custom in-house code, available on GitHub: github.com/bhamla-lab/mudskipper-3D-tracking-ICB-2025.

Directional 3D resolution test using customed USAF-1951 chart

To validate the estimated directional 3D resolution of our stereo camera setup, we conducted a resolution test using a custom-printed USAF-1951 chart. Two GoPro cameras (Hero 10 and Hero 12), previously calibrated and synchronized for field work at 240 fps with 2.7K resolution, were installed on tripods at similar distances (∼1 m) with an angle between lines of sight of ∼120°. The 3D surface of the measurement space in Fig. 5A was calculated using the Gaussian Splatting with commercial software (PolyCam) and calibrated using a letter-sized paper located on the floor at $x = 0$ m, $y = 1.5$ m, $z = 0$ m, which simulates the actual field measurement where the calibration panel is located approximately at the center of both fields of view.

The resolution chart was handheld and manually positioned at different locations within the overlapping field of view. The 3D position of the chart at each location was estimated using Direct Linear Transformation (DLT), i.e., the same technique introduced in Fig. 4F,

based on known camera parameters such as position, orientation, and focal depth (see the three-dimensional locations of symbols in Fig. 5A). In Fig. 5A, the color of each symbol corresponds to the length ratio (R_L) of the reconstructed length of the upper side of the largest square element in the USAF-1951 chart (see Fig. 5B) compared to the actual length. This indicates that length information is most accurate (~97%), where the lines of sight intersect (e.g., $x = 0$ m, $y = 0.5$ m), where mudskipper lengths were measured in general during field research. However, length can be significantly underestimated outside this region, down to ~60%. This error likely stems from severe lens distortion at the edge of the field of view, which could potentially be resolved using higher-order mapping techniques beyond simple DLT and advanced calibration methods such as the Tsai model (Tsai 1987).

Due to the wide field of view, measured resolution varied spatially. To assess directional resolution at each position, the smallest resolvable element visible in the chart was manually recorded for both cameras, and the corresponding resolution in the image plane was estimated in units of mm/pixel using USAF-1951 chart instructions with appropriate scale factors. Measured image-plane resolutions from both cameras in their local x and y directions were projected into world coordinates using each camera's rotation matrix, yielding spatial resolution vectors in x, y, and z directions (Fig. 5C–E).

This estimated spatial resolution along the dominant axes can be obtained from the square roots of eigenvalues of the 3D positional covariance matrix (Σ_X), which is defined as $\Sigma_X = J \cdot \Sigma_{uv} \cdot J^T$, where the diagonal covariance matrix $\Sigma_{uv} \in \mathbb{R}^{4\times4}$ contains squared resolution values in $\mu m^2/pixel^2$ along the diagonal: $\Sigma_{uv} = \text{diag}(r_{1x}^2, r_{1y}^2, r_{2x}^2, r_{2y}^2)$, where r_{ix} and r_{iy} are the measured resolutions of camera i in the image x and y directions. The Jacobian matrix $J \in \mathbb{R}^{3\times4}$ represents the partial derivatives of the reconstructed 3D position, $\mathbf{X}$, with respect to small changes in image coordinates (u_1, v_1, u_2, v_2): $J = \partial\mathbf{X}/\partial(u_1, v_1, u_2, v_2)$. Each element of J was estimated using finite differences by perturbing pixel values by one unit and recalculating the triangulated position using MATLAB in-house code.

Fig. 5C–E clearly demonstrates that resolution varies depending on both the axis and measurement location. In this setup, the highest resolution of 0.27 ± 0.03 mm/pixel was achieved along the z-axis, while the lowest resolution of 0.64 ±0.10 mm/pixel occurred along the x-axis. This corresponds to smallest resolvable spatial patterns of 1.06 mm ±0.11 mm and 2.57 mm ±0.40 mm, respectively, assuming four pixels are required to resolve one pattern. This difference in axial resolution is expected due to the camera angles, as both cameras have their major line-of-sight components along the x-direction. Considering that the minimum mudskipper length exceeds 10 mm, this resolution is sufficient for quantifying fish length. Detailed error analysis of positional accuracy and improvement in directional resolution using enhanced triangulation and calibration techniques will be essential for future studies. The complete implementation, including calibration parsing, Jacobian computation, and resolution visualization, is available at github.com/bhamla-lab/mudskipper-3D-tracking-ICB-2025.

Statistics calculation

The reconstructed 3D trajectory consists of time series data for three position components (x, y, and z over multiple t). Each component is smoothed separately using the built-in smooth function (MATLAB R2022b) with a 15-point moving average, and the velocities in each component are obtained using the central difference method (CD2) via the built-in gradient function (MATLAB R2022b). The velocity shown in Fig. 7A represents the magnitude of the velocity vector, i.e., the norm of the velocity vector. The path length in Fig. 7B is calculated as the sum of the horizontal distances, projected on the xy-plane which is orthogonal to gravity, between adjacent points in the trajectory. The path curvature in Fig. 7E and F is obtained by fitting the trajectory projected onto the horizontal plane to a circle using the least-squares method, and the curvature is obtained by inverting the radius of circle. The stride length in Fig. 7C is defined as the horizontal distance between local minima of the z-coordinate. The stride height in Fig. 7D is defined as the difference between the maximum height and the initial height. The local minima and maxima are determined using the zeros and signs of the first and second derivatives of the vertical position $z(t)$, respectively. A local minimum occurs when $dz/dt = 0$ and $d^2z/dt^2 > 0$, while a local maximum occurs when $dz/dt = 0$ and $d^2z/dt^2 < 0$. The angle in Fig. 7F is defined as the angle between two adjacent trajectory segments, divided by local minima and projected onto the horizontal plane, representing the turning angle between the landing and launching directions at each hopping. We used the sample standard deviation $\sigma = \sqrt{\sum(x - \bar{x})^2/(n-1)}$, where x is each individual data point, $\bar{x}$ is the sample mean, and n is the number of samples.

Results

Representative trajectories

Fig. 6A and B shows three representative 3D trajectories of mudskippers. In both periodic hopping 1 and 2,

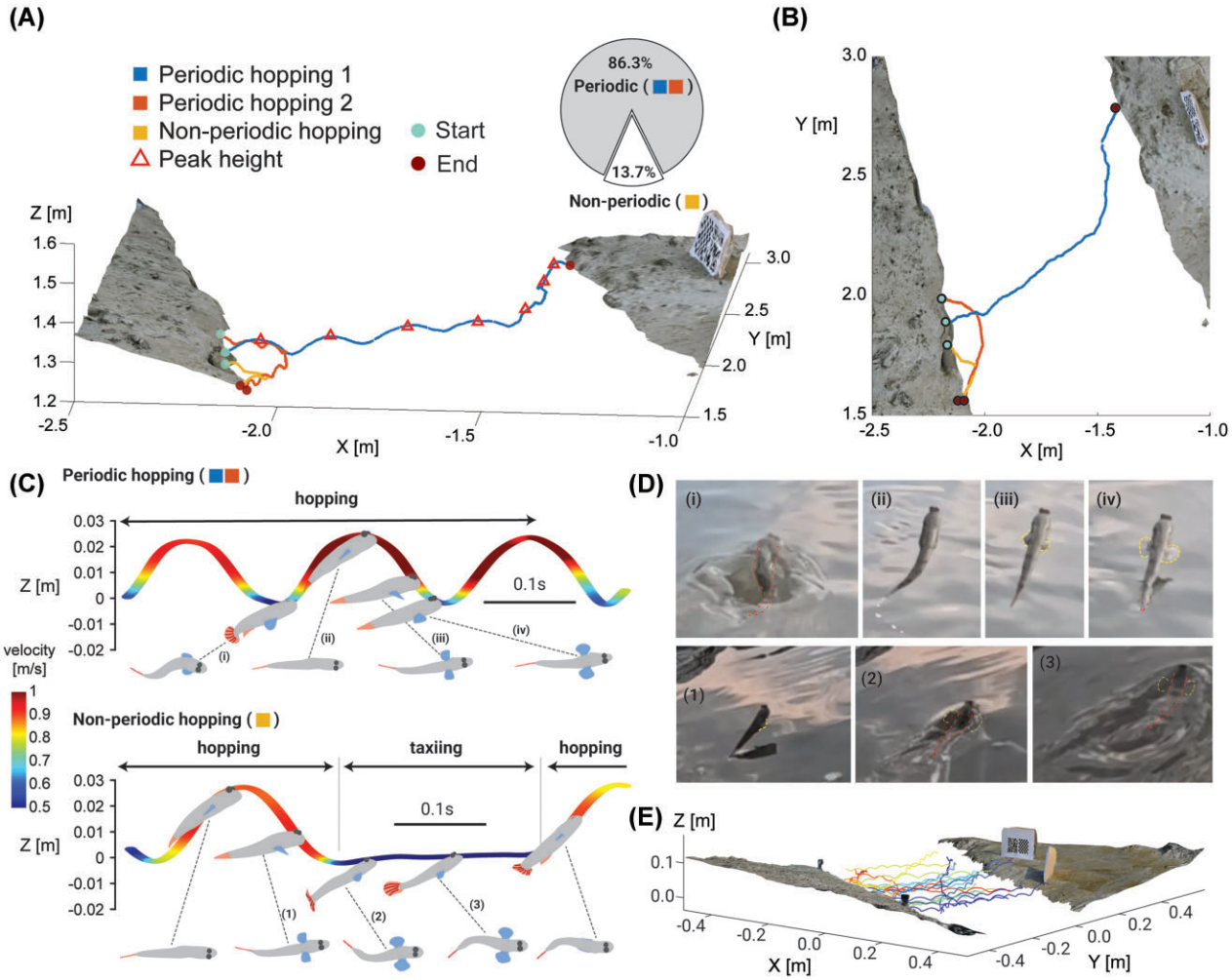

Fig. 6 (**A**) Three representative trajectories of mudskipper paths tracked on the 3D space with reconstructed terrain surface, where "periodic hopping 1" traces a mudskipper traveling across the water from one piece of land to another, the "periodic hopping 2" and "nonperiodic hopping" show mudskippers which traveled onto water but returned back to their starting piece of land. In "nonperiodic hopping," the mudskipper taxied intermittently between hops. The pie chart shows the occurrence rates are 86.3% and 13.7% ($n = 51$) for periodic and nonperiodic trajectories, respectively. (**B**) Top view of the three trajectories. (**C**) Height and velocity over time for two hopping modes: periodic hopping (top) and nonperiodic hopping (bottom). Each schematic illustrates fin and body movements from both the side and top views of the mudskipper. (**D**) Snapshots of fin and body posture during (i–iv) periodic and (1–3) nonperiodic hopping, with indices corresponding to those in (C). Submerged body edges are highlighted with red dotted lines, while fin edges are marked with yellow dotted lines. For taxiing phases (2) and (3), the body and fin outlines are inferred from the authors' observations, as only the eyes are clearly visible. (**E**) Multiple trajectories of mudskipper paths in 3D space for one site.

the mudskippers repeatedly hop above the water surface and make contact with it between hops. The fish either crosses the water, as in periodic hopping 1 with a relatively straighter trajectory, or returns to the same side of land, as in periodic hopping 2 with a more curved path. The top part of Fig. 6C shows the instantaneous velocity during periodic hopping 1, indicating that velocity peaks during each hop and decreases when the fish contacts the water surface. Fin movements are illustrated in the schematics (top part of Fig. 6C) and corresponding snapshots (Fig. 6D*i–iv*). During hopping, the pectoral fins are fully folded and thus nearly invisible, while the caudal fin undulates (Fig. 6C*i–ii* and 7D*i–ii*). As the fish descends, the pectoral fins begin to extend (Fig. 6C*iii* and D*iii*), reaching full extension right just before water contact while the caudal fin becomes idle, as shown in Fig. 6C*iv* and D*iv*.

In nonperiodic hopping (Fig. 6A and B), the fish jumps from land to water, taxis for ∼0.2 s (see the bottom part of Fig. 6C), and then returns to the same land with another hop. Likewise, nonperiodic hopping involves movement that is not solely consecutive hopping but includes "taxiing" before, after, or between hops. Taxiing differs from typical underwater swimming in

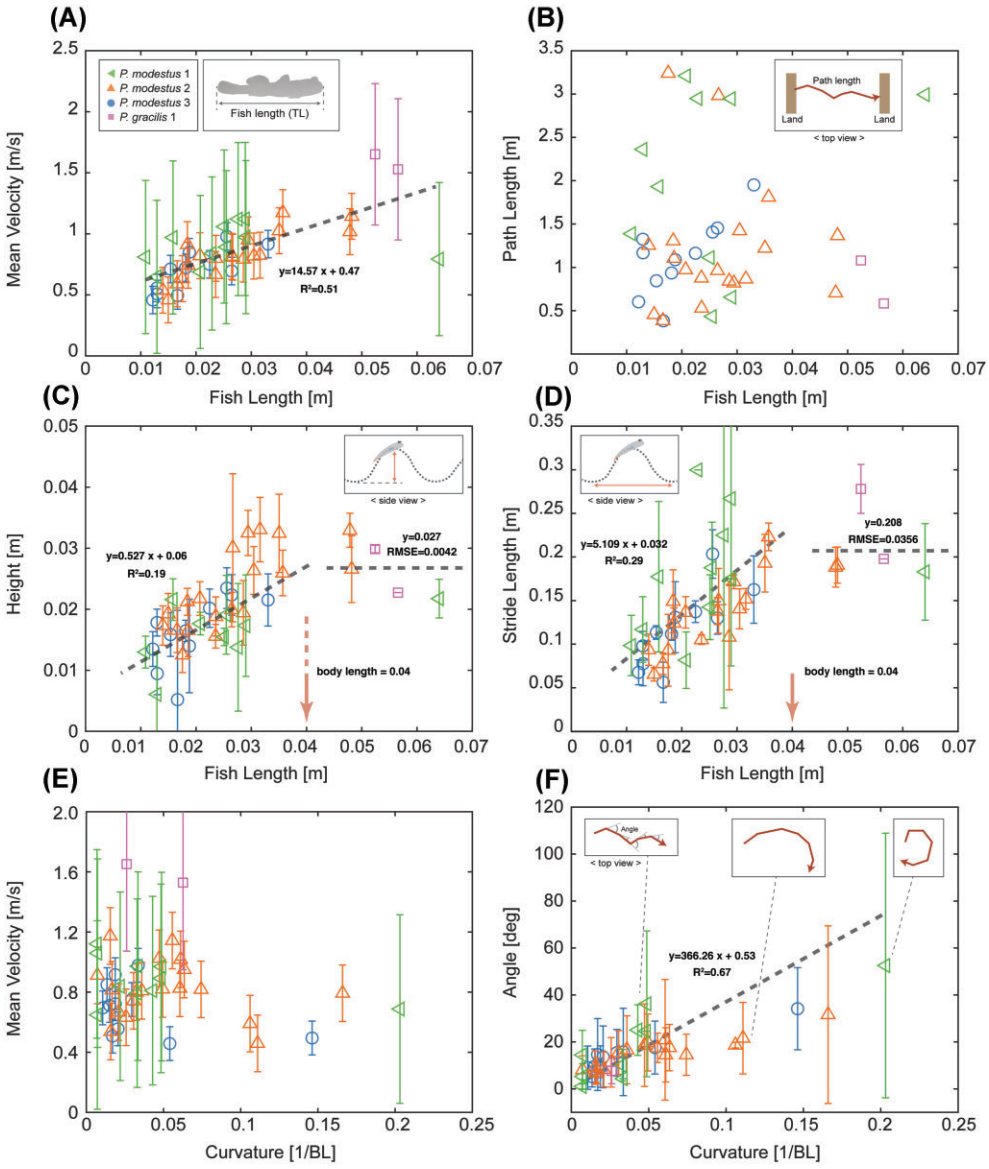

Fig. 7 Statistics of hopping behavior collected from 3D trajectories. (**A**) Mean velocity, (**B**) path length, (**C**) height, and (**D**) stride length as functions of fish length. (**E**) Mean velocity and (**F**) turning angle versus path curvature. Each plot includes 33 trajectories: 31 from South Korea (*P. modestus*) and 2 from Brunei (*P. gracilis*). Error bars indicate sample standard deviation. *P. modestus* 1, 2, and 3 denote different capture locations in Daebudo, Korea.

that most of the fish's body remains submerged, while the eyes stay exposed to air (see schematics of taxiing in the bottom part of Fig. 6C*2–3*). Its fin usage is also distinctive: after water contact, the pectoral fins remain extended to generate lift and keep the body close to the surface while still submerged, while the caudal fin flaps to produce thrust (see Fig. 6C*2–3* and D*2–3*). Due to the extended pectoral fins, high drag may occur, resulting in a low average velocity ($< 0.5 m\,s^{-1}$). We classify these irregularly mixed movement patterns as "nonperiodic hopping." It should be noted that this type of trajectory does not always return to the same shore—it can also involve crossing the water (see Supplementary Video 1, which shows both periodic and nonperiodic trajectories.) A detailed analysis of the biomechanics and fluid mechanics related to fin motion and water surface interaction will be conducted in future work by the authors.

The occurrence rates for periodic and nonperiodic trajectories are 86.3% and 13.7%, respectively ($n = 51$) (see pie chart in Fig. 6A), indicating the fish prefer periodic hopping. Our measurement technique (Fig. 4F) enables estimation of the fish's size by calculating the 3D positions of the edges of the head and tail. Total length (TL) is estimated as $24.6 \pm 10.8\ mm$ ($n = 41$) and $54.5 \pm 2.9\ mm$ ($n = 2$) for *P. modestus* and *P. gracilis*, respectively. Baeck and Park (2015) reported *P. modestus*

in the range of 31–99 mm (TL), which is higher than our measurements, indicating that the mudskippers in our current observations are mostly premature. The length of *P. gracilis* ranges from 25 to 40 mm in standard length (Khaironizam and Norma-Rashid 2002), and its maximum length is comparable to our measurements (noting that our values are in TL), supporting that the observed individuals are fully grown.

Regarding the possibility of species misidentification of *P. modestus*, previous reports indicate that three species of the same genus, *Periophthalmus*, are found in South Korea: *P. modestus* (Lee et al. 1995), *P. magnuspinnatus* (Baeck and Park 2015), and *P. argentilineatus* (Jaafar and Murdy 2017). A distinguishing feature of *P. argentilineatus* is the presence of white dots on the first dorsal fin, while *P. magnuspinnatus* is characterized by sky blue speckles on the head and flank, both of which are absent in the specimen observed in this study (see Fig. 1A). Additionally, the diagnostic traits of *P. modestus* (Jaafar and Murdy 2017), including anteriorly united pelvic fins and a single dusky inframarginal stripe on the dorsal fin, closely match those of our specimen. With these criteria, all mudskippers collected at the site in Daebudo, South Korea, were identified as *P. modestus*.

Statistics analysis

Fig. 7A and B illustrates the mean velocity and the path length of the trajectory as functions of fish body length. The mean velocity increases with body length (Webb 1976; Domenici and Blake 1997), while path length shows low correlation, likely due to the geometry-sensitive nature of water-hopping locomotion. This could be due to the irregular shape of water edge or interruptions caused by land features and dense mangrove roots, which often led to early termination of hopping. In this study, the maximum velocity normalized by body length reached 49.5 BL/s, and the maximum path length covered in a single trajectory was 184.9 BL, both of which are remarkably fast and long. A comparative analysis will be conducted in future work.

Fig. 7C and D presents the vertical height and horizontal stride length for individual hopping segments. A single trajectory may include multiple hopping segments, and each data point represents the mean and standard deviation of each parameter across all segments within one trajectory, corresponding to a single fish of a specific body length. The stride length and vertical height increase linearly with fish body length but begin to plateau beyond a body length of ∼0.04 m. (see the arrows in Fig. 7C and D). When the fish's body length is below 0.04 m, it can jump up to its own body length in height. Horizontally, the mudskipper can leap to about five times its own body length. For mudskippers larger than 0.04 m, both vertical height and horizontal stride lengths tend to remain constant—∼0.027 m and 0.21 m, respectively. The critical limit of 0.04 m likely reflects allometric scaling, where muscle strength and fin area scale as L^2, while body weight scales as L^3. Cano-Barbacil et al. (2020) has reported a critical swimming length limit of ∼0.1 m for freshwater fish (Cano-Barbacil et al. 2020), probably suggesting mudskippers face additional energetic costs from overcoming gravity during water-hopping. Further biomechanical analysis and additional hopping data from larger individuals are needed to confirm this scaling relationship.

Lastly, Fig. 7E and F presents the mean velocity as a function of curvature and the change in horizontal angle (in the z-plane) between hopping segments. From Fig. 7F, the mean velocity is hardly affected by small curvature below $0.1\,BL^{-1}$ after which mean velocity is significantly decreased $< 1\,m\,s^{-1}$. We can infer that for more curved trajectories ($> 0.1\,BL^{-1}$), part of the horizontal momentum is lost before the next leap, and assuming the same energy expenditure, this leads to lower overall velocity. In addition, mudskippers can adjust the horizontal angle between each hopping segment in proportion to the curvature (Fig. 7F). It should be noted that mudskippers appear to adjust turning angles between hops in response to predators or terrain, indicating sophisticated sensorimotor control that enables real-time trajectory adjustments during escape. Future studies of the neural and biomechanics mechanisms underlying this flexibility could reveal how mudskippers integrate sensory feedback with locomotor control during water-hopping.

Discussion

Comparisons with other amphibious organisms

The relationship to other water-surface traveling animals can be made by utilizing dimensionless parameters such as the Bond, Reynolds, and Weber numbers for each animal. Values and definitions for these numbers can be found in Table 2. These numbers were calculated using the mean estimated TL of *P. modestus* as the characteristic length, D, and the mean velocity, v, was estimated from the trend line in Fig. 7A, with horizontal and vertical components denoted by subscripts H and V, respectively. These components were obtained by assuming an incoming body angle of 30° relative to the horizontal plane of the water surface. The other parameters, ρ, ν, and σ, all correspond to the density, kinematic viscosity, and surface tension of water at standard temperature and pressure, and g is the gravitational constant near the surface of the earth. Comparing the

Table 2 Dimensionless numbers (Bond, Weber, and Reynolds) definition and value given measurements recorded using proposed method.

Dimensionless number	Definition	*P. modestus* value
Bond	$\rho g D/\sigma$	8.21×10^{1}
Horizontal Weber	$\rho v_H^2 D/\sigma$	1.99×10^{2}
Vertical Weber	$\rho v_V^2 D/\sigma$	6.62×10^{1}
Horizontal Reynolds	$v_H D/\nu$	1.87×10^{4}
Vertical Reynolds	$v_V D/\nu$	1.08×10^{4}

Bond number to the Weber numbers and the respective Reynolds numbers to Weber numbers shows that the mudskipper closely aligns with the relationships of dimensionless quantities for water walkers suggested by Bush and Hu, Fig. 5 and 6 in Bush and Hu (2006) (not shown here), in the horizontal direction and loosely aligns in the vertical. The significance of this is that Froude's Law applies to *P. modestus* as well and it can be classified as a water-walker. Additionally, the high Weber number means that the main forces experienced by the mudskipper are the inertial and buoyant forces.

The mudskipper kinematics observed here, in contrast to data from laboratory mudskippers (Swanson and Gibb 2004) and amphibious animals such as frogs (Weiss 2023) or the plumed basilisk lizard (Hsieh 2003), can help elucidate the limits of water-surface traversal mechanisms. Here, water-surface traversal mechanisms refer to locomotion techniques where the only forces aiding the movement are from the water surface interface. Weiss (2023) indicates that the skittering frog follows a primarily ballistic trajectory, reaching a maximum velocity of ∼1.1 m/s, and the basilisk is reported to run at about 1.3 m/s (Hsieh 2003). These velocities are similar to the mudskippers mean velocity, which may suggest that water-surface traversal methods may have a maximum velocity limit, somewhere between 1.5 and 2 m/s. This claim is further reinforced by the water strider, *Gerridae*, which is reported to have peak velocities of 1.5 m/s as well (Hu et al. 2003). As for length scales, the Snout-vent lengths of the basilisk and skittering frog are on the order of 0.1 m (Laerm 1974; Hsieh 2003), while water striders and mudskippers (studied here) have characteristic lengths on the order of 0.01 m (Hu et al. 2003). Based on the data reviewed here, this limit may only apply to length scales on orders of 0.01 or 0.1 m. The reason behind this suggested limit is currently unknown, but it may be due to an increase in the hydrodynamic drag, and an increase in the energy dispersal through water as velocities increase. Other animals, such as the flying fish *Exocoetidae*, also with characteristic lengths on the order of 0.1 m, are seen breaking this limit at ∼15–20 m/s (Davenport 1994), although since they generate lift with their fins they experience forces outside of the air water interface, and the proposed limit would not apply since it would not be bound to the water surface to propel or sustain its movement.

Convergent evolution in water-surface hopping

Interesting comparisons can be drawn between the mudskippers' water-hopping behavior and other organisms that have adapted to hop on water, such as the Chinese rice grasshopper, *Oxya chinensis*, and Pygmy mole crickets, *Xya capensis*. Although not closely related to the mudskipper, both insects can hop on water, often repeatedly (Burrows and Sutton 2012; Song et al. 2024). Both mudskippers and the insects use a caudal structure to propel themselves out of the water. The grasshopper and crickets use their hind legs, and the mudskipper uses its caudal fin. This mechanism often functions as an escape from predators. This similarity can be seen as a convergent evolution, and deeper investigations may have significant implications for bio-inspired designs featuring adaptable, multimodal locomotion. Such designs could address diverse environmental scenarios, including muddy, wet, and uneven surfaces (as seen in the mudskipper), flight (as in the grasshopper), flooding and burrowing (as in the cricket), and the common link of hopping to escape via water.

Evidence for ballistic motion

Our imaging analysis indicates that the mudskipper's parabolic hops resemble the ballistic motion observed in the African Butterfly Fish (Saidel et al. 2004) and the skittering frog (Weiss 2023), albeit with a distinct take-off mechanism. The African Butterfly Fish uses an abduction of its fins to propel itself upward (Saidel et al. 2004), whereas the skittering frog does a standard jump but in the water (Weiss 2023), and the mudskipper launches itself by rapidly straightening its caudal fin, previously bent into a C-shape (Wicaksono et al. 2020). Despite differing modes of propulsion, all follow a similarly parabolic path.

Saidel et al. (2004) identify several criteria characterizing ballistic motion in the African Butterfly Fish; our findings align with five of their points:

(1) The mudskipper's short take-off period occurs when the fish bends its caudal fin and quickly extends it.
(2) A single peak in the path is evident in the trajectory data.
(3) Stride length spans a few body lengths (as shown in Fig. 5D).

(4) Velocities remain below those of flying fish *Exocoetidae* (15–20 m/s) (Davenport 1994).
(5) The observed path is parabolic.

There is insufficient data to confirm the sixth criterion of short air time compared to flying fish. However, the parabolic arc suggests no significant gliding: the mudskipper's time aloft is notably shorter than flying fish, indicating ballistic motion, rather than sustained flight.

Directional preference as an escape mechanism

The high frequency of smaller curvatures, corresponding to turning angles $< 40°$, suggests that mudskippers typically move in a single direction with minimal veering. This may be because altering the course could lead back toward the original danger, introduce new danger, or require more energy. Consequently, this locomotion is consistent with an escape mechanism, as noted by Harris (1960), although Davenport observed that flying fish sometimes employ flying to reach food sources (Davenport 1994). Overall, water hopping in mudskippers operates as a multifunctional traversal method, yet its out-of-water motion follows a predominantly ballistic trajectory, distinct from the sustained flight of other species.

Limitation and application of the proposed method

This method requires four major constraints.

(1) The camera position must remain fixed during recording. It cannot be placed on any surface that moves, such as a vessel in motion or a swaying tree branch.
(2) The observer must have sufficient accessibility to collect enough snapshots of the terrain on which the organism moves. In this study, mudskippers lived in a creek that reached only thigh depth or in shallow puddles entirely surrounded by land, allowing multiple-angle snapshots. If such viewpoints are not possible, other measures need to be explored.
(3) The target organisms must stay within or return to the field of view after setup and snapshot acquisition. Although the mudskippers tended to move away from observers due to their sensitivity, their very high density ensured they were always present in the observation area. Otherwise, one would need either less invasive methods for snapshots or other techniques for terrain measurement.
(4) Organisms must be optically visible, as tracking becomes difficult, for example, when they frequently dive or hide in burrows. Mudskippers, however, typically keep their eyes exposed while hopping, making this method feasible for their observation.

When these conditions are met, the proposed approach offers high temporal resolution (e.g., 4.2 ms in this study) and high spatial resolution (e.g., 0.5 mm) over a broad observation domain (e.g., $1.5 \times 1.5 \times 1$ m). For instance, water striders ~50 mm in size, found in the same habitat as *P. modestus*, were also observed hopping across the water surface and traveling distances exceeding 2 m at velocities of about 1 m/s. Their three-dimensional movement could be adequately captured with this technique. This approach is not limited to centimeter-scale organisms. By rearranging the camera placement, for instance on exposed rocks at the ocean's edge, it becomes feasible to measure three-dimensional movements over tens of meters, including sea otters swimming at the water surface or pelicans hunting while floating, as well as the relationships between these animals and surrounding terrain. Terrestrial and aerial organisms, such as rabbits moving on land or insects flying and hopping, could also be observed provided the terrain is captured from multiple angles in the limited time. This method is particularly effective in situations where the observer must operate in random and unpredictable terrain, or when filming needs to be completed within a short time frame.

It is necessary to discuss potential errors in organism positioning caused by inaccuracies in the camera's intrinsic and extrinsic parameters. This method adjusts the camera's position, orientation, and focal length by manually matching the real camera view with the reconstructed terrain's virtual camera view. Future refinements using advanced techniques, such as cross-correlation (Lucas and Kanade 1981) based on light intensity and color information in the reconstructed terrain, or methods such as Shake-the-Box (Schanz et al. 2016) and auto-calibration (Theriault et al. 2014), could further automate and enhance this calibration process, which is expected to improve the overall methodology.

Conclusion

This study presents the first comprehensive three-dimensional analysis of mudskipper water-hopping behavior in natural habitats, revealing fundamental biomechanical principles that govern amphibious locomotion at the air–water interface. Through our portable, dual-camera tracking system combined with Gaussian Splatting terrain reconstruction, we quantified complex locomotory patterns that were previously inaccessible.

Our findings demonstrate that mudskipper hopping follows predictable scaling relationships, with both horizontal stride length and vertical height increasing lin-

early with body size up to a critical threshold of ~0.04 m TL. Beyond this limit, performance plateaus, suggesting biomechanical constraints that may reflect the balance between muscle power scaling and gravitational forces. The discovery of two distinct hopping modes, i.e., periodic and nonperiodic, reveals sophisticated behavioral flexibility that enables mudskippers to navigate complex tidal environments. The predominance of periodic hopping (86.3% of observed trajectories) and the strong directional preference during escape responses underscore the adaptive significance of this locomotory strategy for predator avoidance and habitat exploitation. The dimensional analysis shows that mudskipper water-hopping can be classified as water-walking and reveals alignment with the dimensionless relationships of other water-walking organisms from different taxonomic groups.

The methodological framework developed in this study is applicable beyond mudskipper biology. Our low cost (under $1500), field deployable approach (within 25 min) enables high resolution 3D tracking in natural environments where traditional laboratory setups are impractical. The quantitative approach established here offers a foundation for comparative studies across amphibious species and may inform engineering insights inspired by multimodal locomotion. By integrating field-based tracking with precise biomechanical analysis, this study helps bridge the gap between laboratory research and natural behavior, contributing to a more comprehensive understanding of locomotor adaptation in complex environments.

Author contributions

D.C. conceived, conducted experiments, analyzed the results, wrote, and reviewed the manuscript. K.Y. obtained, anaylzed tracking data, wrote, and reviewed the manuscript. H.W. obtained the tracking data. I.B. discussed fish behavior and wrote the manuscript. U.G. organized and helped field work. S.B. supervised projects, wrote, and reviewed the manuscript.

Acknowledgments

We thank the Universiti Brunei Darussalam for our Research Collaboration Approval and Agreement UBD/AVC-RI/1.21.1[a]/2024/009 and the Royal Brunei Yacht Club for supplying their resources. We thank members of the Bhamla Lab for helpful discussions, Nami Ha, Immanuel John, Joremy Tony, Katrin Grafe for their collaboration during field work, Akshay Sivakumar for preparing the equipment and Dr. Pankaj Rohilla for his valuable feedback and mentorship. Text in this paper was revised using ChatGPT-4 and Claude Sonnet 4. Animal procedures were approved by Georgia Tech IACUC (Protocol BHAMLA-A100704). The field work in South Korea (Brunei) has been conducted at 27th August 2024 (29th August 2024) and the location is 37°15′N 126°33′E (4°58′N 115°03′E).

Funding

S.B. acknowledges funding support from NSF Grants CAREER iOS-1941933, PHY-2310691 and Schmidt Sciences, LLC. D.C. acknowledges funding support from the National Research Foundation of Korea (NRF) grant funded by the Ministry of Science and ICT (RS-2023-00248034) and the 2024 Nerem Travel Award from the Petit Institute for Bioengineering and Bioscience at Georgia Institute of Technology.

Supplementary Data

Supplementary data available at *ICB* online.

Conflict of interest

No competing interest is declared.

Data availability

The datasets supporting the conclusions of this article are available in the GitHub repository at github.com/bhamla-lab/mudskipper-3D-tracking-ICB-2025. This repository includes the custom MATLAB code for 3D trajectory reconstruction, camera calibration scripts, stereo matching algorithms, representative trajectory data, and all data supporting the statistical analyses presented in Figs. 5 and 7. Raw video files and complete datasets generated during field studies are available from the corresponding author upon reasonable request due to large file sizes.

References

3D Polycam Inc, 2024. Polycam. [Mobile Application]. https://poly.cam

Baeck GW, Park JM. 2015. Length–weight and length–length relationships and seasonal condition factors for two mudskippers, *Periophthalmus modestus* (Cantor, 1842) and *P. magnuspinnatus* (Lee, Choi and Ryu, 1995) (Gobiidae), on tidal flats of Korea. J Appl Ichthyol 31:261–4. https://doi.org/10.1111/jai.12655

Burrows M, Sutton GP. 2012. Pygmy mole crickets jump from water. Curr Biol 22:R990–1. https://10.1016/j.cub.2012.10.045

Bush JW, Hu DL. 2006. Walking on water: biolocomotion at the interface. Annu Rev Fluid Mech 38:339–69. https://doi.org/10.1146/annurev.fluid.38.050304.092157.

Cano-Barbacil C, Radinger J, Argudo M, Rubio-Gracia F, Vila-Gispert A, García-Berthou E. 2020. Key factors explaining critical swimming speed in freshwater fish: a review and statistical analysis for Iberian species. Sci Rep 10:18947. https://doi.org/10.1038/s41598-020-75974-x.

Davenport J. 1994. How and why do flying fish fly? Rev Fish Biol Fish 4:184–214. https://doi.org/10.1007/BF00044128.
Domenici P, Blake RW. 1997. The kinematics and performance of fish fast-start swimming. J Exp Biol 200:1165–78. https://doi.org/10.1242/jeb.200.8.1165.
Fan X, Wang X, Ni H, Xin Y, Shi P. 2025. Water-adapted 3D gaussian splatting for precise underwater scene reconstruction. Front Mar Sci 12:1573612. https://doi.org/10.3389/fmars.2025.1573612.
Francisco FA, Nührenberg P, Jordan A. 2020. High-resolution, non-invasive animal tracking and reconstruction of local environment in aquatic ecosystems. Mov Ecol 8: 1–12. https://10.1186/s40462-020-00214-w
Glasheen JW, McMahon TA. 1996. Size-dependence of water-running ability in basilisk lizards (*Basiliscus basiliscus*). J Exp Biol 199:2611–8. https://doi.org/10.1242/jeb.199.12.2611.
Harris VA. 1960. On the locomotion of the mud-skipper *Periophthalmus koelreuteri* (Pallas): (Gobiidae). Proc Zool Soc Lond 134:107–35. https://doi.org/10.1111/j.1469-7998.1960.tb05921.x.
Hedrick TL. 2008. Software techniques for two- and three-dimensional kinematic measurements of biological and biomimetic systems. Bioinspir Biomim 3:034001. https://doi.org/10.1088/1748-3182/3/3/034001.
Hsieh ST. 2003. Three-dimensional hindlimb kinematics of water running in the plumed basilisk lizard (*Basiliscus plumifrons*). J Exp Biol 206:4363–77. https://doi.org/10.1242/jeb.00679.
Hu DL, Chan B, Bush JWM. 2003. The hydrodynamics of water strider locomotion. Nature 424:663–6. https://doi.org/10.1038/nature01793.
Ikebe Y, Oishi T. 1996. Correlation between environmental parameters and behaviour during high tides in *Periophthalmus modestus*. J Fish Biol 49:139–47. https://10.1111/j.1095-8649.1996.tb00010.x
Jaafar Z, Murdy EO. 2017. Fishes out of water: biology and ecology of mudskippers. In: CRC marine science. Boca Raton, FL, USA: CRC Press.
Kerbl B, Kopanas G, Leimkühler T, Drettakis G. 2023. 3D Gaussian splatting for real-time radiance field rendering. ACM Trans Graph 42:139–1. https://10.1145/3592433
Khaironizam MZ, Norma-Rashid Y. 2002. Length–weight relationship of mudskippers (Gobiidae:Oxudercinae) in the coastal areas of Selangor, Malaysia. Naga WorldFish Cent Q 25:20–2.
Laerm J. 1974. A functional analysis of morphological variation and differential niche utilization in basilisk lizards. Ecology 55:404–11. https://doi.org/10.2307/1935228.
Lee TH, Choi Y, Ryu JB. 1995. A taxonomic revision of the genus *Periophthalmus* (Pisces:Gobiidae) from Korea with description of a new species. Kor J Ichthyol 7: 39–45.
Liu S, Huang B, Qian F. 2023. Adaptation of flipper-mud interactions enables effective terrestrial locomotion on muddy substrates. IEEE Robot Autom Lett 8:7978–85. https://doi.org/10.1109/LRA.2023.3323123.
Lucas BD, Kanade T. 1981. An iterative image registration technique with an application to stereo vision. Proceedings of the Seventh International Joint Conference on Artificial Intelligence . 81. p. 674–9, New York, USA.
Macnae W. 1969. A general account of the fauna and flora of mangrove swamps and forests in the Indo–West-Pacific region. In: Russell FS, Yonge M. editors. Advances in marine biology. Academic Press, vol. 6, p. 73–270.
Naylor ER, Kawano SM. 2022. Mudskippers modulate their locomotor kinematics when moving on deformable and inclined substrates. Integr Comp Biol 62:1335–56. https://doi.org/10.1093/icb/icac084.
Pace CM, Gibb AC. 2009. Mudskipper pectoral fin kinematics in aquatic and terrestrial environments. J Exp Biol 212:2279–86. https://doi.org/10.1242/jeb.029041.
Petit MG. 1921. Observations sur certains poissons des côtes de Madagascar, présentant une adaptation à la locomotion terrestre. Bull Mus Hist Nat 27:216–20.
Rosellini L, Hersen F, Clanet C, Bocquet L. 2005. Skipping stones. J Fluid Mech 543:137–46. https://doi.org/10.1017/S0022112005006373.
Saidel WM, Strain GF, Fornari SK. 2004. Characterization of the aerial escape response of the African butterfly fish, *Pantodon buchholzi* Peters. Environ Biol Fishes 71:63–72. https://doi.org/10.1023/B:EBFI.0000043153.38418.cd.
Schanz D, Gesemann S, Schröder A. 2016. Shake-the-box: Lagrangian particle tracking at high particle image densities. Exp Fluids 57:70. https://doi.org/10.1007/s00348-016-2157-1.
Song Y, Wang H, Dai Z, Ji A, Wu H, Gorb SN. 2024. Multiple forces facilitate the aquatic acrobatics of grasshopper and bioinspired robot. Proc Natl Acad Sci USA 121:e2313305121. https://doi.org/10.1073/pnas.2313305121.
Stebbins RC, Kalk M. 1961. Observations on the natural history of the mud-skipper, *Periophthalmus sobrinus*. Copeia 1961:18–27. https://10.2307/1440166
Swanson BO, Gibb AC. 2004. Kinematics of aquatic and terrestrial escape responses in mudskippers. J Exp Biol 207:4037–44. https://doi.org/10.1242/jeb.01237.
Theriault DH, Fuller NW, Jackson BE, Bluhm E, Evangelista D, Wu Z, Betke M, Hedrick TL. 2014. A protocol and calibration method for accurate multi-camera field videography. J Exp Biol 217:1843–8. https://10.1242/jeb.100529
Tsai RY. 1987. A versatile camera calibration technique for high-accuracy 3D machine vision metrology using off-the-shelf TV cameras and lenses. IEEE J Robot Autom 3:323–44. https://doi.org/10.1109/JRA.1987.1087109.
Vieira M, Guedes Soares C, Guimarães PV, Bergamasco F, Campos RM. 2025. Nearshore space-time ocean wave observation using low-cost video cameras. Coast Eng 197:104694. https://doi.org/10.1016/j.coastaleng.2024.104694.
Webb PW. 1976. The effect of size on the fast-start performance of rainbow trout Salmo gairdneri and a consideration of piscivorous predator–prey interaction. J Exp Biol 65:157–77. https://doi.org/10.1242/jeb.65.1.157.
Weiss TM. 2023. Locomotion of skittering frogs at the air-water interface [dissertation]. Virginia Polytechnic Institute and State University.
Wicaksono A, Hidayat S, Retnoaji B, Alam P. 2020. The water-hopping kinematics of the tree-climbing fish, *Periophthalmus variabilis*. Zoology 139:125750. https://10.1016/j.zool.2020.125750